

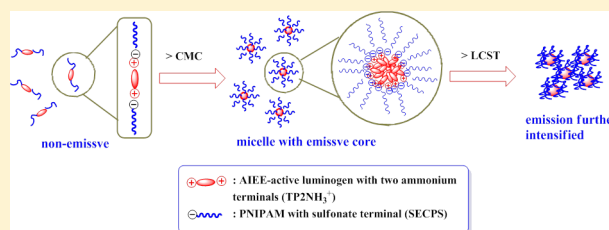
# Complexation of Fluorescent Tetraphenylthiophene-Derived Ammonium Chloride to Poly(*N*-isopropylacrylamide) with Sulfonate Terminal: Aggregation-Induced Emission, Critical Micelle Concentration, and Lower Critical Solution Temperature

Chih-Min Yang, Yi-Wei Lai, Shiao-Wei Kuo, and Jin-Long Hong\*

Department of Materials and Optoelectric Science, National Sun Yat-Sen University, Kaohsiung, Taiwan 80424

## Supporting Information

**ABSTRACT:** Amphiphilic polymers with hydrophilic poly(*N*-isopropylacrylamide) (PNIPAM) shell connecting hydrophobic tetraphenylthiophene (TP) core, which has the novel aggregation-induced emission (AIE) property, by ionic bonds were prepared to explore the AIE-operative emission responses toward critical micelle concentration (CMC) and lower critical solution temperature (LCST). To exercise the idea, ammonium-functionalized TP2NH<sub>3</sub><sup>+</sup> and sulfonate-terminated PNIPAM were separately prepared and mixed in different molar ratios to yield three amphiphilic TP-PNIPAM<sub>*n*</sub> complexes for the evaluations of CMC and LCST by fluorescence responses. The nonemissive dilute aqueous solutions of TP-PNIPAM<sub>*n*</sub> became fluorescent when increasing concentrations above CMC. Heating micelles solution to temperatures above LCSTs causes further enhancement on the emission intensity. The fluorescence responses are explained by the extent of aggregation in the micelles and in the globules formed at room temperature and at high temperatures, respectively.



## 1. INTRODUCTION

Polymer micelles<sup>1</sup> responsive to external stimuli have received considerable research interest due to their potential applications on drug delivery<sup>2</sup> and catalysis.<sup>3</sup> Among them, amphiphilic block copolymer is one attractive system and much effort<sup>4</sup> has been directed toward engineering “smart” micelle from the hydrophilic/hydrophobic polymers featuring multiple-stimuli. In water, the amphiphilic block copolymers are aggregated to form different molecular assemblies by the repelling and coordinating action between the hydrophilic and hydrophobic parts to the surrounding environment. At low concentrations, copolymers in aqueous solutions exist as individual molecules; their self-assembly starts when copolymer concentration reaches the specific value of critical micelle concentration (CMC). Previous study on the amphiphilic poly(ethylene glycol)-*b*-poly(*L*-lactide) (PEG-PLLA),<sup>5</sup> polystyrene-*b*-poly(ethylene oxide),<sup>6</sup> and polycarbonate-*b*-poly(*N*-isopropylacrylamide) (PC-PNIPAM)<sup>7</sup> has suggested that CMC depends strongly on the chemical nature and the ratio between the hydrophilic and the hydrophobic blocks. With the higher PLLA/PEG ratio, the corresponding PEG-PLLA<sup>5</sup> tends to form micelles with a lower CMC.

In addition to CMC, the thermally induced conformational change of PNIPAM also stimulated much research interest.<sup>8–13</sup> Under semidilute conditions, PNIPAM in water forms a clear solution that rapidly clears, becomes cloudy upon heating to temperatures above 32 °C, the lower critical solution temperature (LCST). A possible model relating to the

corresponding coil-to-globule collapse of PNIPAM in water<sup>14–16</sup> has been proposed and the temperature-driven single-chain conformational transformation and the subsequent macroscopic phase separation reflect rather subtle changes in polymer/water hydrogen-bond (H-bond) interactions, primarily the release of water molecules from a polymer hydrophilic layer into the bulk water. Minor changes in the chemical composition of PNIPAM were anticipated to have significant influences on the phase diagram of PNIPAM in water.<sup>16</sup>

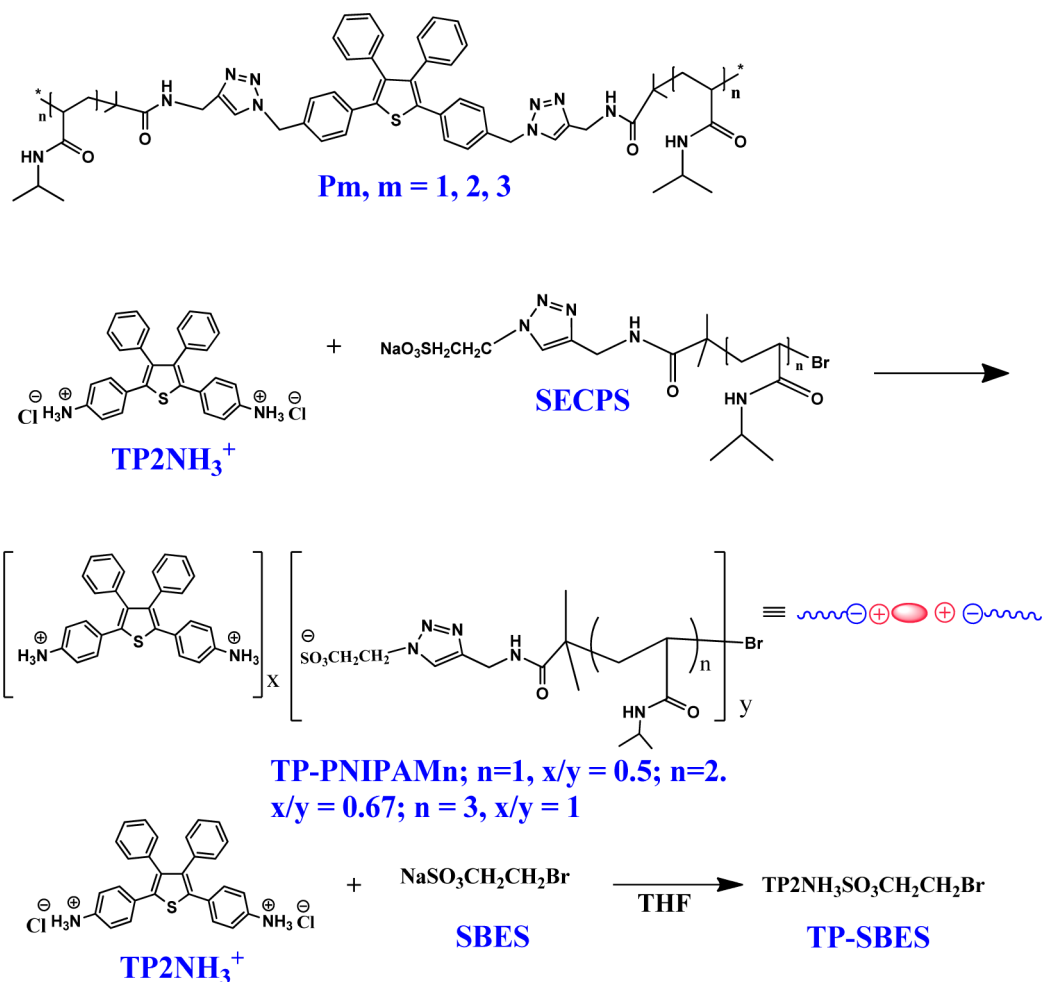
Conventional organic luminogens enjoy the high fluorescence in the dilute solutions but suffer from the detrimental aggregation-caused quenching (ACQ) in the concentrated solution and solid states. When dispersed in liquid media or fabricated into solid film, the fluorescence of conventional luminogens is often weakened or even quenched, which greatly limits their real-world application. In 2001, Tang’s group discovered that one particular silole molecule (1-methyl-1,2,3,4,5-pentaphenylsilole) emits strongly in the concentrated solution or the solid state even though it is nonemissive in the dilute solution.<sup>17</sup> This interesting phenomenon was designated as “aggregation-induced emission” (AIE) later on to emphasize the phenomenon that the originally nonemissive solution of silole can be tuned to emit strongly when the corresponding aggregates formed after introduction of the water nonsolvent.

Received: September 20, 2012

Revised: October 16, 2012

Published: October 17, 2012

Scheme 1. Chemical Structures of Covalently-Bonded TP Polymers of  $P_m$  and Mixings of  $TP2NH_3^+$  with SECPS and SBES To Prepare Ionic Complexes of  $TP$ -PNIPAM $_n$  and  $TP$ -SBES, Respectively



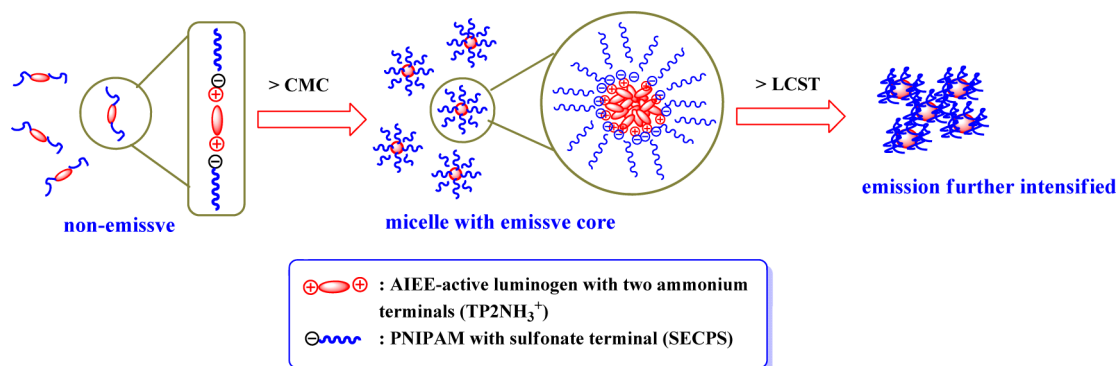
The AIE effect is rationalized as a result of restricted intramolecular rotation (RIR) of the phenyl peripheries<sup>18–21</sup> against the central silole core in the aggregate state. It was rationalized that the nonradiative channel via the vibrational/torsional energy relaxation processes can be blocked in the aggregate state, leading to the enhanced radiative recombination of the excited state. Since the first discovery of the silole system, several organic and polymeric materials<sup>22–37</sup> with AIE or AIE enhancement (AIEE) properties have been prepared and well characterized.

Luminescence spectroscopy is a useful technique in the investigations of the thermal response of PNIPAM<sup>10–13</sup> due to the distinguished sensitivity. Generally, labeling with trace amounts of fluorescent materials allows major examination of the transformations between intra- and intermolecular interactions. In this way, PNIPAM copolymers with an AIE-active tetraphenylthiophene (TP) center<sup>36</sup> ( $P_m$ , Scheme 1) were previously synthesized in our laboratory to approach LCST with AIE-related fluorescence. In water medium, micelles from the TP-derived PNIPAM emit strongly due to the aggregated TP core but at temperatures above LCST the collapse of micelles results in the dissociated TP core and isolation of TP luminogens by the retracted PNIPAM chains causes the emission quenching; therefore, a fluorescence responsive system based on the switch of intra- to intermolecular interactions was created.

Instead of the covalent bond used in  $P_m$ , ionic  $TP$ -PNIPAM (Scheme 1) was also developed in our lab and was found to form core-shell micelles<sup>37</sup> in water. By adjusting the complexation ratio between the TP-derived ammonium dication ( $TP2NH_3^+$ ) and the sulfonate-terminated anion (PNIPAM- $SO_3^-$ ), the resultant ionic complexes of  $TP$ -PNIPAM $_n$  self-assemble into micelles with the ionic ammonium sulfonate ( $-NH_3^+O_3S^-$ ) bonds as the interconnecting units between the TP core and the PNIPAM shell layers. Under the operations of acid, base, and metal ions,<sup>37</sup> the ionic ammonium sulfonate bonds can be ruptured to result in the collapse of micelles and the concurrent dissociation of the aggregated TP core results in the observed emission reduction; therefore, the ionic  $TP$ -PNIPAM complexes serve as fluorogenic sensor capable of responding to acid, base, and metal ions.

Analogous to the amphiphilic PC-PNIPAM<sup>7</sup> block copolymer, the ionic  $TP$ -PNIPAM $_n$  ( $n = 1, 2$ , and 3 with varied  $x/y$  (= molar ratio between  $TP2NH_3^+$  and PNIPAM chain)) complexes also have a similar hydrophobic/hydrophilic chemical architecture. However, the non-site-specific interactions involved in between the charged aromatic  $TP2NH_3^+$  cation and the charged sulfonate counteranions are similar to the long-range electrostatic interactions involved in lots of aromatic dye/nonaromatic polyelectrolyte<sup>38–44</sup> (PEL) systems. Study on one specific example of  $TP$ - $NH_3^+$ /poly(vinyl

**Scheme 2. Schematic Illustrations for Self-Assembled Micelles Structure of TP-PNIPAM<sub>n</sub> above Critical Micelles Concentration (CMC) and the Subsequent Global Micelles Aggregation at Temperatures above LCST**



sulfonate)<sup>44</sup> (PVS) developed in our lab indicated that the AIE-active TP-NH<sub>3</sub><sup>+</sup> luminogens self-assemble into emissive aggregates stabilized by the long-range electrostatic forces from the phase-separated PVS counteranions. The non-site-specific long-range interactions stabilize the aggregated TP-NH<sub>3</sub><sup>+</sup> phase; likewise, we expect the same type of stabilization forces in the present TP-PNIPAM<sub>n</sub> system.

By adjusting the amounts of TP2NH<sub>3</sub><sup>+</sup> and PNIPAM-SO<sub>3</sub><sup>-</sup>, three TP-PNIPAM<sub>n</sub> complexes with varied hydrophobic to hydrophilic  $x/y$  ratios were prepared in our lab in order to study the interrelationship of AIE-operative luminescence to CMC and LCST: as illustrated in Scheme 2, in water, the TP-PNIPAM<sub>n</sub> chains below CMC are separated and dispersed by the water molecules and in this case, the fluorescent TP-NH<sub>3</sub><sup>+</sup> units are supposed to emit weakly (or nonemissive) due to the inoperative AIE property. However, at concentrations above CMC, micelles with core-shell morphology form and the aggregated TP core inside the micelles is expected to emit intensely because of the AIE effect exerted by the aggregated luminogens. The fluorescence response toward concentration of the aqueous TP-PNIPAM solution therefore can be utilized to locate CMC. At temperatures above LCST, coil-to-globule collapse of PNIPAM occurs and the temperature-driven single-chain conformational transformation and the concurrent macroscopic phase separation reflect rather subtle changes in polymer/water hydrogen-bonded interactions. In addition, the lone-range electrostatic forces involved in the present system should play a role on the integrity and the stability of the phase-separated TP2NH<sub>3</sub><sup>+</sup> domains inside the globular structure. The AIE-operative emission response across LCST will in turn reflect the possible morphological change at high temperatures. Control on the hydrophobic to hydrophilic ratio ( $x/y$ ) will give micelles of different CMCs and LCSTs. The interrelationship between AIE-operative luminescence, CMC, and aggregated core morphology above LCST is the focus of this study.

## 2. EXPERIMENTAL SECTION

**Preparation of TP-PNIPAM<sub>n</sub> Complexes.** Different amounts of TP2NH<sub>3</sub>Cl<sup>37</sup> compounds were dissolved in 5 mL of THF and added to a solution of SECPS<sup>37</sup> (7.2 g; 2.04 mmol) in THF (5 mL). The precipitates after addition were then filtered and dried under vacuum to obtain the desired products of TP-PNIPAM<sub>n</sub> (cf. Table 1 for the detailed composition). TP-PNIPAM1 ( $x/y = 1/2$ ):  $T_g = 144$  °C; TP-PNIPAM2 ( $x/y = 1/1.51$ ):  $T_g = 141$  °C; TP-PNIPAM3 ( $x/y = 1/1$ ):  $T_g = 137$  °C; selected spectral data for TP-PNIPAM1: IR (KBr pellet, cm<sup>-1</sup>) 3440, 3298, 3071, 2971, 2933, 2874, 1651, 1541, 1460, 1388, 1358, 1258, 1171, 1127, 1115; <sup>1</sup>H NMR (500 MHz, CDCl<sub>3</sub>)  $\delta$  6.95–7.24 (m, 18H, aromatic Hs), 6.11–6.87 (broad, 2H, NHCO), 5.29 (s,

**Table 1. Molecular Weights of SECPS and TP-PNIPAM<sub>n</sub> Evaluated from MALDI-TOF Mass, <sup>1</sup>H NMR Spectra, and UV-Vis Spectra**

sample	from MALDI-TOF				$x/y^b$		
	$M_n^a$	$M_w^a$	PDI <sup>a</sup>	$x/y^b$	from <sup>1</sup> H NMR	from UV-vis	from feed ratio
SECPS	3000	3500	1.19				
TP-PNIPAM1	7200	7500	1.04	0.5	0.5	0.5	0.49
TP-PNIPAM2	5200	5700	1.08	0.67	0.68	0.68	0.66
TP-PNIPAM3	3600	3900	1.08	1.01	1.03	1.04	1.00

<sup>a</sup> $M_n$  = number average molecular weight,  $M_w$  = weight-average molecular weight, PDI = polydispersity. <sup>b</sup> $x/y$  = the molar ratio between TP2NH<sub>3</sub><sup>+</sup> fluorophore and PNIPAM chain; evaluated from <sup>1</sup>H NMR, MALDI-TOF, and UV-vis spectra and from the applied recipes in the experimental preparative step.

6H, H<sub>k</sub>), 4.01 (broad, 1H, CH(CH<sub>3</sub>)<sub>2</sub>), 3.75 (t, 2H, H<sub>l</sub>), 3.49 (t, 2H, H<sub>g</sub>), 1.4–2.2 (broad, 3H, backbone Hs), 1.18 (broad, 6H, CH(CH<sub>3</sub>)<sub>2</sub>) (Figure 1).

**Instrumentation.** UV-vis absorption spectra were recorded with an Ocean Optics DT 1000 CE 376 spectrophotometer. FL spectra were obtained from a LabGuide X350 fluorescence spectrophotometer, using a 450W Xe lamp as the continuous light source. Quantum efficiencies ( $\Phi_F$ ) of solid samples were measured in an integrating sphere made by Ocean Optics. For liquid solutions, values of  $\Phi_F$ s were obtained by using quinine sulfate as reference standard (10<sup>-4</sup> M in 0.1 N H<sub>2</sub>SO<sub>4</sub>). <sup>1</sup>H NMR spectra were recorded with a VarianVXR-500 MHz FT-NMR instrument. Tetramethylsilane was used as internal standard. FT-IR spectra were obtained on a Bruker Tensor 27. Particle sizes of TP-PNIPAMs in ethanol/acetone mixtures were measured by dynamic light scattering (DLS), using a Brookhaven 90 plus spectrometer equipped with a temperature controller. An argon ion laser operating at 658 nm was used as the light source. A mass spectrum was obtained by using a Bruker Daltonics Autoflex III MALDI-TOF mass spectrometer. The glass transition temperature ( $T_g$ ) of the polymer were determined from a TA Q-20 differential scanning calorimeter (DSC) with a scan rate of 20 deg/min under nitrogen. TEM was obtained from a JEM-2100 electron microscope with LaB<sub>6</sub> as the light source.

## 3. RESULTS AND DISCUSSION

**Primary Characterizations on TP-PNIPAM<sub>n</sub> Complexes.** According to Scheme 1, three TP-PNIPAM<sub>n</sub> complexes with varied hydrophobic TP to hydrophilic PNIPAM ratios were prepared by mixing different amounts

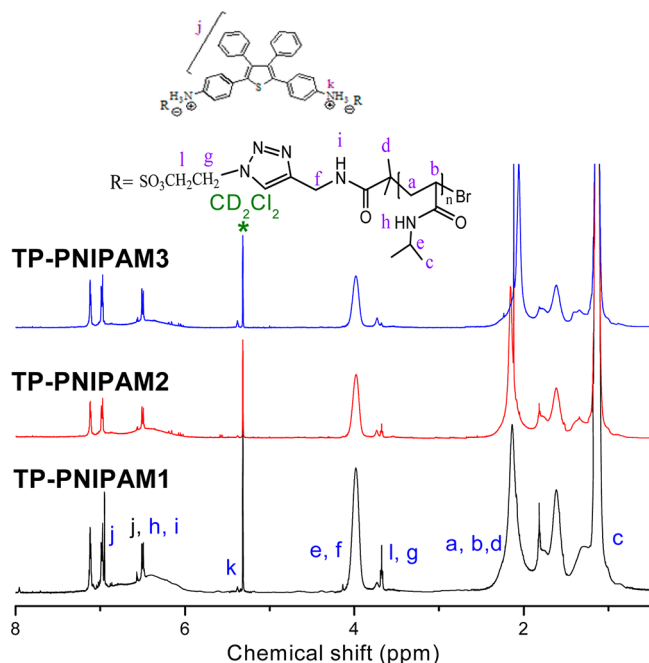


**Figure 1.**  $^1\text{H}$  NMR spectra of TP-PNIPAM1, TP-PNIPAM2, and TP-PNIPAM3 ( $\text{CD}_2\text{Cl}_2$ ).

of  $\text{TP}2\text{NH}_3^+$  with SECP polymer in the preparative solution state. According to the MALDI-TOF mass spectra (Figure S1), the key precursor SECPS<sup>37</sup> prepared in our lab has a degree of polymerization (DP) of 28, which is slightly lower than that ( $\approx 31$ ) calculated from the  $^1\text{H}$  NMR spectrum. With the terminal sulfonate anion, SECP readily reacts with the two ammonium groups in  $\text{TP}2\text{NH}_3^+$ ; after reaction, the number of hydrophobic  $\text{TP}2\text{NH}_3^+$  incorporated per each hydrophilic PNIPAM chain (as the hydrophobic to hydrophilic ratio ( $\approx x/y$ )) in the resultant TP-PNIPAMs can be evaluated from the MALDI-TOF mass, the  $^1\text{H}$  NMR, and the UV-vis absorption spectra. The resultant  $x/y$  ratio, the corresponding number- and weight-average molecular weights ( $M_n$  and  $M_w$ ), and polydispersity (PDI) of all polymers and complexes are summarized in Table 1.

The  $^1\text{H}$  NMR spectra give primary characterizations on the hydrophobic to hydrophilic molar ratio of  $x/y$ . As shown in Figure 1, the integration ratio of the aromatic proton ( $\text{H}_j$ ), the amino  $-\text{NH}$  proton ( $\text{H}_i + \text{H}_h$ ), and the methylene proton ( $\text{H}_f + \text{H}_g$ ) resonances can be used to formulate  $M_n$  and the  $x/y$  ratio, which are correlated well with the values obtained from the MALDI-TOF mass spectra. Besides  $^1\text{H}$  NMR and MALDI-TOF mass, the UV-vis absorption spectra are also used to evaluate the  $x/y$  ratios.

To serve as external standard of the UV-vis spectra, the TP-SBES compound ( $\text{TP}2\text{NH}_3\text{SO}_3\text{CH}_2\text{CH}_2\text{Br}$ , cf. Scheme 1) was prepared from complexation reaction between  $\text{TP}2\text{NH}_3^+$  and  $\text{NaSO}_3\text{CH}_2\text{CH}_2\text{Br}$  (SBES). The solution absorption peak of the TP-SBES solution locates at the same position of 344 nm as that of the TP-PNIPAM solutions, which suggests that the built-in TP luminogen is indeed the real absorption species responsible for TP-SBES and the TP-PNIPAMs, too. As illustrated in Figure 2, the solution absorbance of TP-SBES and TP-PNIPAMs solutions at 344 nm can be linearly proportional to their concentration. According to Beer-Lambert law, the molar absorption coefficient ( $\epsilon$ ) from the calibration curve of TP-SBES is  $0.2462 \text{ L}/(\text{mol}\cdot\text{cm})$ , which can be further used to

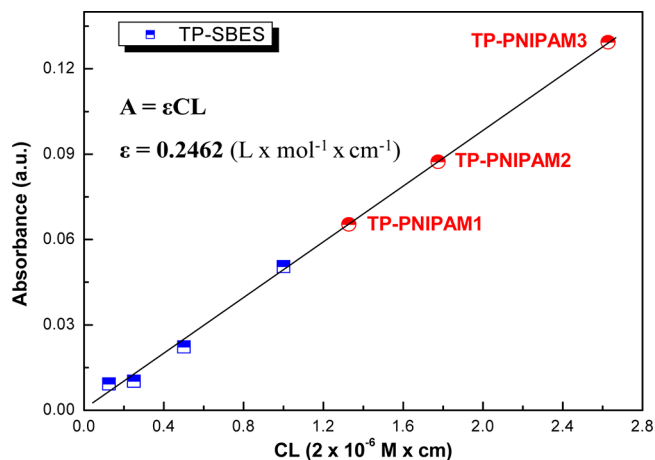


**Figure 2.** Calibration curve for dilute solutions of TP-PNIPAM $n$  and  $\text{TP}2\text{NH}_3\text{SO}_3\text{CH}_2\text{CH}_2\text{Br}$  (TP-SBES) in THF. Absorbance at 344 nm was recorded and concentrations of TP-SBES and TP-PNIPAM $n$  are in the ranges of  $0.125 \times 10^{-5}$  to  $10^{-5}$  M and  $1.39 \times 10^{-5}$  to  $2.78 \times 10^{-5}$  M in THF, respectively. (A: absorbance;  $\epsilon$ : molar absorption coefficient; C: concentration; and L: thickness of the sample cell.)

evaluate the corresponding  $M_n$  of TP-PNIPAM. As illustrated in Table 1, the resolved  $x/y$  ratios based on the UV-vis absorption spectra are well correlated with those from the  $^1\text{H}$  NMR, the MALDI-TOF spectra, and the feed ratio applied in the preparative mixing step, which indicates that the complexation reaction between ammonium cation and sulfonate anion proceeds thoroughly to result in the complete formation of the ammonium-sulfonate bond. From TP-PNIPAM1 to TP-PNIPAM3, the hydrophobic to hydrophilic  $x/y$  ratio increases from 0.5 to 1.

**AIE Property of TP-PNIPAM.** Characterizations on the AIE property of the amphiphilic TP-PNIPAM complexes are conducted in ethanol/acetone solvent/nonsolvent pair. Beforehand, certain solubility behavior of  $\text{TP}2\text{NH}_3^+$  should be clarified. With the two ionic ammonium functions, the highly aromatic  $\text{TP}2\text{NH}_3^+$  molecule is still insoluble in hydrophilic solvents such as methanol and ethanol. Therefore, successful complexation between  $\text{TP}2\text{NH}_3^+$  to SECPS can be demonstrated by the homogeneous dispersion of TP-PNIPAM $n$  in ethanol. The TEM image (Figure S1, Supporting Information) of the solid TP-PNIPAM1 cast from ethanol solution actually confirms the formation of micelles particles. DLS analyses (Figure 3A–C) on the solution mixtures suggest that nanoparticles with average hydrodynamic diameters ( $D_h$ s) of 220 to 370 nm (Figure 3D) formed when TP-PNIPAMs were dispersed in ethanol/acetone of different volume fractions. For all solutions, addition of acetone nonsolvent results in the continuous shrinkage of the nanoparticles. Suggestively, the particles reduce their sizes in order to prevent the included hydrophobic  $\text{TP}2\text{NH}_3^+$  from the acetone nonsolvent. With the highest hydrophobic content, solutions of TP-PNIPAM3 contain particles with the smallest sizes among all solutions with the same volume fractions. This volume shrinkage changes the AIE-operative emission behavior as discussed next.

The fundamental features of AIE-operative emission that the fluorescence emission intensity increases with increasing nonsolvent acetone content in the solutions are observed in all three TP-PNIPAM $n$  solution systems (Figure 4A–C). The resolved monomer and aggregate emissions at the short- and long-wavelength regions are well correlated with the emission

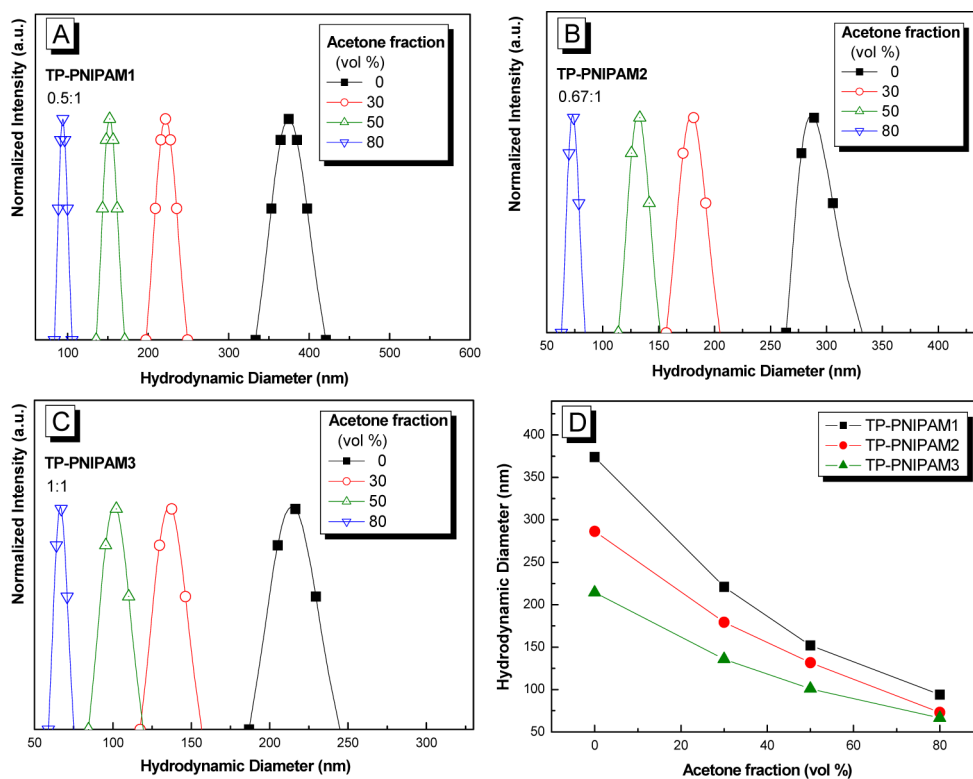


**Figure 3.** Histograms of (A) TP-PNIPAM1, (B) TP-PNIPAM2, and (C) TP-PNIPAM3 ( $10^{-5}$  M) in ethanol/acetone mixtures of different acetone composition and (D) the summarized average hydrodynamic diameter ( $D_h$ ) of all micelles formed by TP-PNIPAM $n$ .

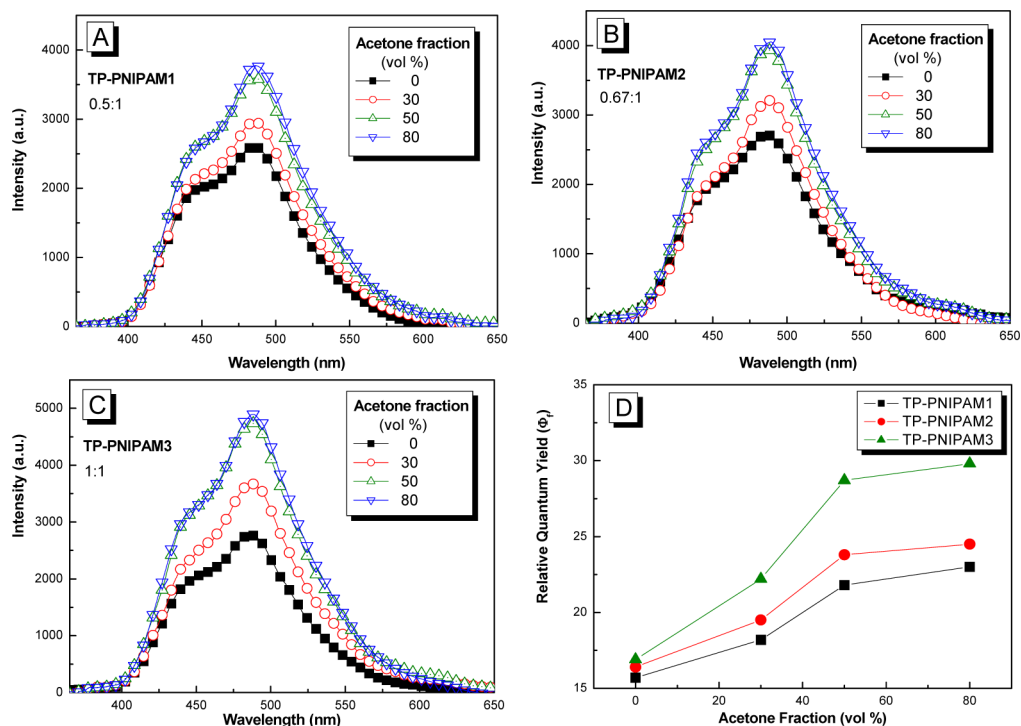


**Figure 4.** Fluorescence emission spectra of (A) TP-PNIPAM1, (B) TP-PNIPAM2, and (C) TP-PNIPAM3 ( $10^{-5}$  M) in ethanol/acetone mixtures of different volume fractions ( $\lambda_{ex} = 350$  nm) and (D) the summarized  $\Phi_F$  values for all mixture solutions.

spectra<sup>37</sup> of the model TP2NH<sub>3</sub><sup>+</sup> solutions. In pure ethanol, all TP-PNIPAM $n$  solutions already exert appreciable emission intensity, which is attributed to the aggregated TP luminogens in the micelle particles. Addition of acetone results in the emission intensifications as illustrated by the resultant solution

quantum yields ( $\Phi_F$ ) summarized in Figure 4D. The TP-PNIPAM3 solutions have the highest emission intensity among all three systems. As suggested by the DLS results in Figure 3, the inclusion of acetone nonsolvent causes the shrinkage of the nanoparticles in the solutions. Molecular rotations of the

TP2NH<sub>3</sub><sup>+</sup> luminogens are increasingly restricted in the shrunk particles under the constraints imposed by the congested environment. Nanoparticles from TP-PNIPAM3 have the smallest dimensions among all three (cf. Figure 3), leading to the effective restrictions on the molecular rotations and the corresponding enhanced emission due to the blockage of the nonradiative decay channels.

**CMC of TP-PNIPAM<sub>n</sub> in Water.** In water with a concentration above CMC, the amphiphilic TP-PNIPAM chains can self-assemble into micelles with core-shell morphology according to our previous study.<sup>37</sup> The aggregated TP2NH<sub>3</sub><sup>+</sup> luminogens in the core region should exert strong AIE-operative emission but at concentrations below CMC, the TP2NH<sub>3</sub><sup>+</sup> species in the dilute solution are isolated from each other and no emission is expected in this case. Indeed, all TP-PNIPAM<sub>n</sub> solutions are nonemissive below CMC and at concentrations above CMC the resolved emission intensities of all three TP-PNIPAM<sub>n</sub> solutions (Figure 5A) can be attributed

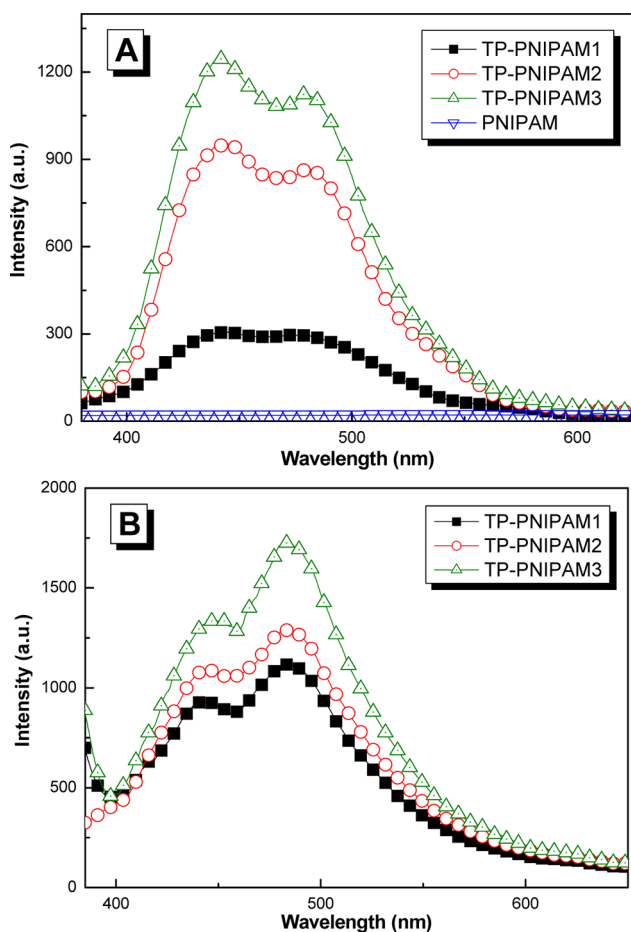


**Figure 5.** (A) Solution emission spectra of TP-PNIPAM<sub>n</sub>s ( $6.676 \times 10^{-5}$  M) and PNIPAM ( $2.779 \times 10^{-4}$  M) in water and (B) the solid emission spectra of TP-PNIPAM<sub>n</sub> ( $\lambda_{\text{ex}} = 350$  nm).

to the inherent TP2NH<sub>3</sub><sup>+</sup> species since pure PNIPAM solution is virtually nonemissive. In accord with the inherent luminogen content, the aqueous TP-PNIPAM3 solution emits with the highest emission intensity among all three.

Fluorescence spectra of solid samples cast from the aqueous solutions are examined in Figure 5B. In the aspect of limited mobility in the condensed state, the solid samples all exhibit higher emission intensity than the mother aqueous solutions.

Morphology of the solid film is reminiscent of the mother solution and in resemblance to the solutions solid TP-PNIPAM3 also shows the highest emission intensity (Figure 5B) among all three solids. Quantum yields obtained from integrating sphere support this result with the resolved values of 28%, 31%, and 37% for TP-PNIPAM1, -2, and -3, respectively.

The response of the AIE-operative fluorescence behavior toward the concentration of the aqueous TP-PNIPAM solutions was used to locate the CMC. Here, the aggregate emission (at 484 nm) due to the aggregated TP2NH<sub>3</sub><sup>+</sup> luminogens was used to track the CMC values and the intensity of the aggregate emission was plotted against the solution concentration in Figure 6A–C. At low concentrations below CMC, the detected intensity of aggregate emission is nil or low but at concentrations above CMC the aggregate emission increases abruptly. With the highest hydrophobic content, TP-PNIPAM3 has the lowest CMC ( $=0.068$  mg/mL) as compared to the respective values of 0.105 and 0.139 mg/mL resolved for TP-PNIPAM2 and TP-PNIPAM1. The result is reasonable because the hydrophobic TP units will force the TP-PNIPAM3 chain to form micelles at the stage earlier than those of TP-PNIPAM2 and TP-PNIPAM1 with less hydrophobic content. The resolved values can be qualitatively compared to previous results: the copolymeric system of poly(*N*-vinylpyrrolidone)-*b*-PNIPAM<sup>45</sup> (PVR-*b*-PNIPAM) with  $\sim 76$  wt % of PNIPAM content has a smaller CMC value of 0.026 mg/mL, which is conceivable because the long hydrophobic PVR chains tend to associate with each other more easily than the present system with a small-mass hydrophobic core.

Previous work<sup>46</sup> on ionic liquid of *N*-alkyl-*N*-methylpyrrolidinium bromide (*C<sub>n</sub>MPB*) showed that the logarithmic CMC ( $\log$  CMC) is linearly proportional to the carbon number of the *N*-alkyl chain in *C<sub>n</sub>MPB*. Instead of the carbon number employed in *C<sub>n</sub>MPB*, the hydrophobic fraction ( $=x/(x+y)$ ) was used to correlate with  $\log$  CMC. It can be found in Figure 6D that  $\log$  CMC decreases linearly with the increase of  $x/y$ , following the empirical Stauff–Klevens rule<sup>47</sup> below:

$$\log \text{CMC} = A - B(x/y)$$

The values of constants *A* and *B* evaluated from Figure 6D are 0.24 and 1.87, respectively. A smaller value of *A* or a larger value of *B* implies that micelle formation is more favorable. In comparison to the values ( $A = 1.72$  and  $B = 0.3$ ) obtained from *C<sub>n</sub>MPB*, we may suggest that the polymeric TP-PNIPAM<sub>n</sub> system has a higher tendency to form micelles than the small-mass *C<sub>n</sub>MPB*. The long PNIPAM chains of TP-PNIPAM<sub>n</sub> tend to self-assemble to each other at an earlier stage than the small-mass *C<sub>n</sub>MPB*. In addition, the aromatic rings of TP2NH<sub>3</sub><sup>+</sup> are supposed to be more hydrophobic than the aliphatic chains of *C<sub>n</sub>MPB*, which contributes to the observed lower CMC of TP-PNIPAM<sub>n</sub> as compared to *C<sub>n</sub>MPB*.

**LCST of TP-PNIPAMs.** The thermal induced collapse/aggregation process of the PNIPAM chains across LCST should affect the molecular aggregation and the corresponding absorption and emission behaviors of the TP2NH<sub>3</sub><sup>+</sup> luminogens in TP-PNIPAM<sub>n</sub> complexes. The UV–vis absorption and the fluorescence spectra of the aqueous TP-PNIPAM<sub>n</sub> solutions at room temperature and at 55 °C ( $>$ LCST) are examined in Figure 7, parts A and B, respectively. At room temperature, the absorbance of the aqueous TP-PNIPAM<sub>n</sub> solutions increases with the increasing luminogen content in the samples, which is reasonable in considering that the TP

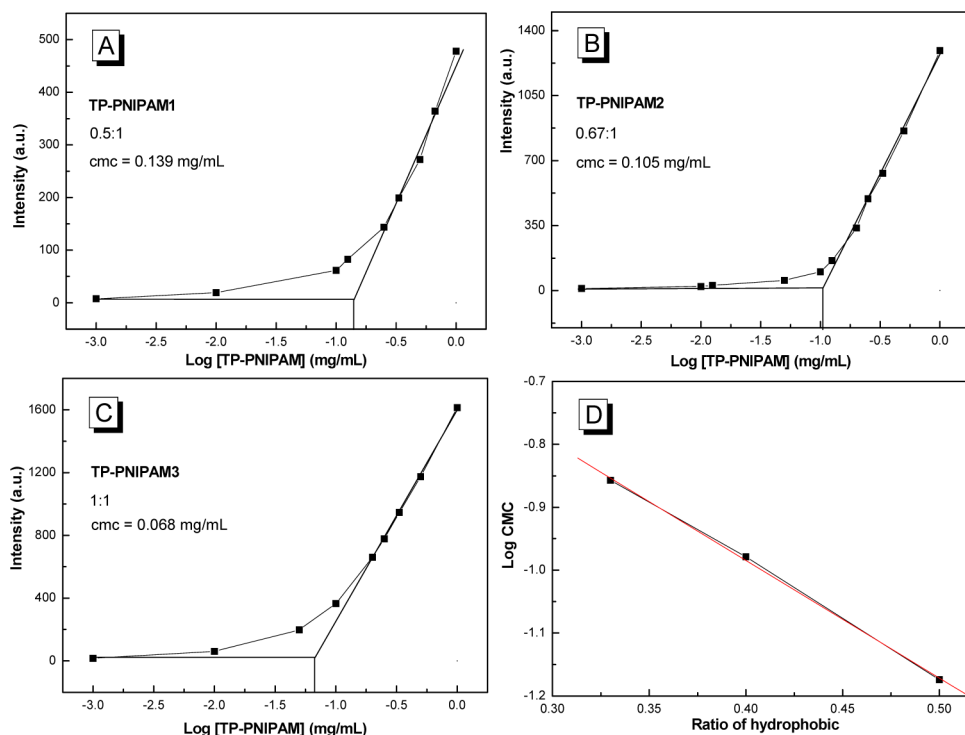


**Figure 6.** (A–C) Intensity of the aggregate emission vs the logarithm of the concentration of TP-PNIPAM $n$  ( $\lambda_{\text{ex}} = 350$  nm,  $\lambda_{\text{em}} = 484$  nm) and (D) linear relationship of log CMC vs molar fraction ( $= x/(x + y)$ ) of the hydrophobic TP $2\text{NH}_3^+$ .

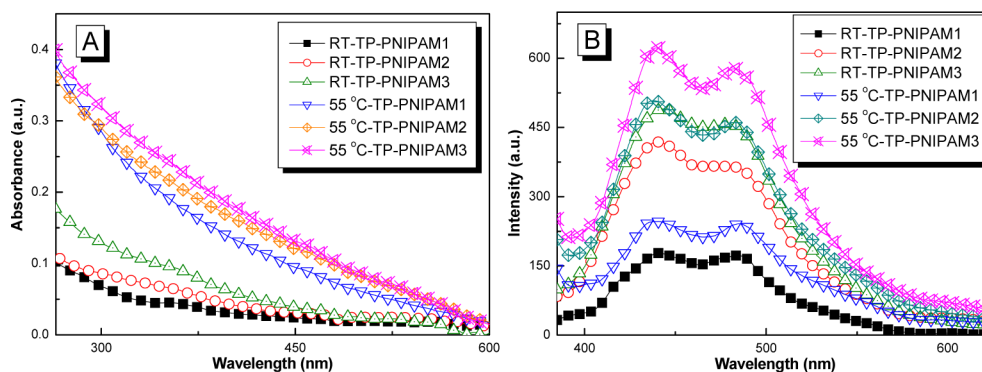


**Figure 7.** (A) Absorption and (B) emission ( $\lambda_{\text{ex}} = 350$  nm) spectra of the aqueous TP-PNIPAM1, TP-PNIPAM2, and TP-PNIPAM3 ( $6.676 \times 10^{-5}$  M) solutions at room temperature and at 55 °C.

luminogens are the main absorbing species responsible for the spectra. The absorbances in all spectra resolved at 55 °C are larger than those at room temperature and most noticeably, the absorptions actually extended over 500 nm. These long-wavelength tails are attributed to the Mie scattering by the large particles formed during the macroscopic aggregation process at temperatures greater than LCST. The DLS analysis given next will further verify the presence of large nanoparticles at high temperatures. For all three TP-PNIPAM $n$  solutions, the emission intensities resolved at 55 °C (Figure 7B) are comparatively higher than their respective counterparts at room temperature. The emission spectra were then deconvoluted into monomer and aggregate bands by curve-fitting and the resultant band areas were integrated to obtain the fractions of the monomer and aggregate emissions (as  $f_M$  and  $f_A$ ). The results summarized in Table 2 indicate that the ratios of  $f_A/f_M$  at 55 °C are all higher than those at room temperature. In considering that AIE-oriented emission is related to the extent

**Table 2.** The Resolved Fractions of Monomer and Aggregate Emissions at Room Temperature and at 55 °C

sample	$f_M^a$ (%)	$f_A^b$ (%)	$f_A/f_M$
TP-PNIPAM1 at RT	49.0	51	1.06
TP-PNIPAM1 at 55 °C	46.2	54.8	1.16
TP-PNIPAM2 at RT	48.6	52.0	1.07
TP-PNIPAM2 at 55 °C	47.0	53.0	1.13
TP-PNIPAM3 at RT	48.0	52.0	1.08
TP-PNIPAM3 at 55 °C	44.2	55.8	1.26

<sup>a</sup>Area fraction of the monomer emission band. <sup>b</sup>Area fraction of the aggregate emission band.

of aggregation of the fluorescence species, we speculate here that further aggregations of the TP $2\text{NH}_3^+$  luminogens occur at high temperatures above LCST. At high temperatures, further aggregation may generate TP $2\text{NH}_3^+$  luminogens with less molecular mobility than when at room temperature.

Optical transmittances and average hydrodynamic diameter ( $D_h$ ) of all three aqueous solutions are monitored in the temperature range of 40–56 °C (Figure 8). Here, transmittance

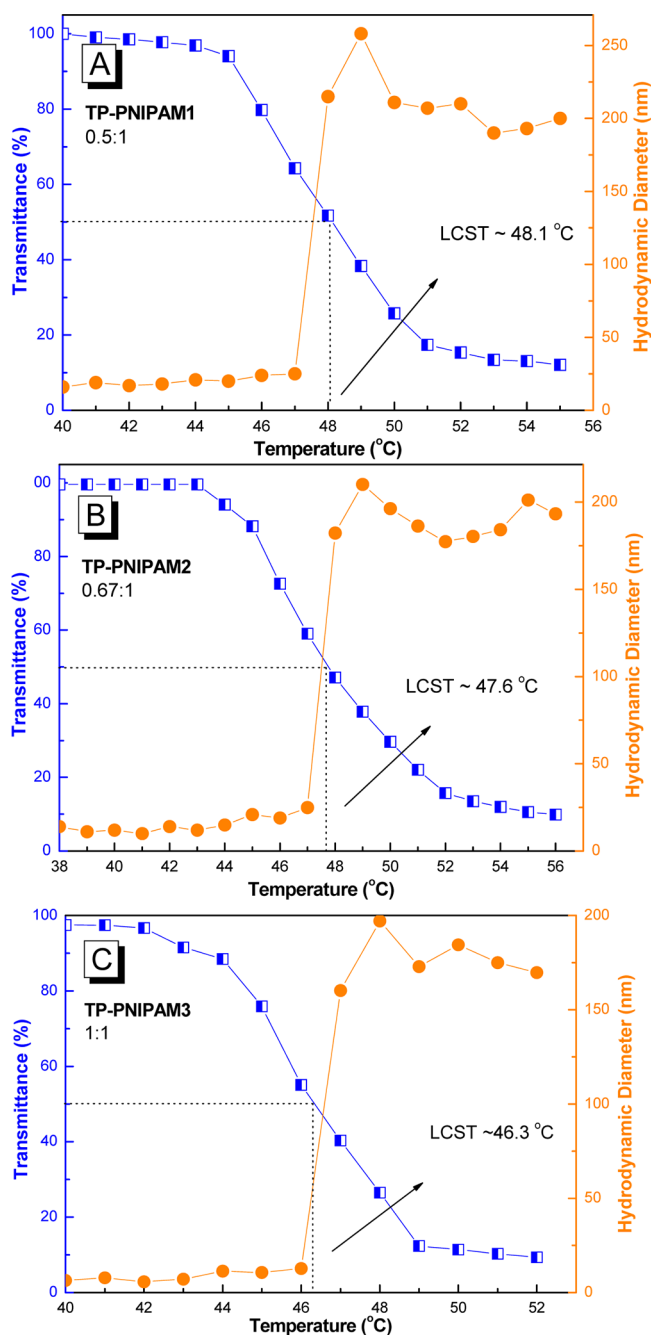


**Figure 8.** Transmittance (blue line, monitored at 680 nm) and hydrodynamic diameter (orange line) vs temperature for the aqueous (A) TP-PNIPAM1, (B) TP-PNIPAM2, and (C) TP-PNIPAM3 solutions ( $3.338 \times 10^{-5}$  M).

was measured at the particular wavelength of 680 nm to avoid possible interferences from the fluorescent species. For all sample solutions, transmittance decreases drastically when heated to temperatures near 44 °C and approaches nil at temperatures >52 °C. The sudden transmittance fall in the temperature range of 44–51 °C indicates that further aggregations of the originally formed micelles proceeded, forming large nanoparticles capable of scattering incident light

efficiently to result in solutions with high opaqueness. The macroscopic aggregation process above LCST can be evidenced by the corresponding variations of the resolved  $D_h$  values in the same temperature ranges: the resolved  $D_h$ s for all sample solutions are relatively constant and small below 46 °C but beyond that, the corresponding  $D_h$ s increase drastically until the final leveling-off in the range of 170–200 nm at 55 °C. The high  $D_h$  values detected at >LCST are essentially different from the small micelle dimensions (<10 nm) at room temperature; therefore, further aggregation of several originally formed micelles into large globular particles with  $D_h > 170$  nm occurs.

The LCSTs detected by transmittance measurement are 48.1, 47.6, and 46.3 °C for TP-PNIPAM1, -2, and -3, respectively. The introduction of the hydrophobic TP2NH<sub>3</sub><sup>+</sup> luminogen tends to lower the affinity of the amphiphilic polymers toward the surrounding water molecules; as a result, TP-PNIPAM3 complex with the highest TP2NH<sub>3</sub><sup>+</sup> content has the lowest LCST among all three solutions.

To collect more information about chain conformation of TP-PNIPAM $n$  and to gain more insight into the thermal transitions, the <sup>1</sup>H NMR spectra are measured in solvents of different affinities and at different temperatures. When in a good solvent like CD<sub>2</sub>Cl<sub>2</sub>, the <sup>1</sup>H NMR spectrum (Figure 9A) of the selected TP-PNIPAM1 shows the resonance signals of all aromatic protons ( $H_j$ ) in the TP2NH<sub>3</sub><sup>+</sup> luminogen and in the PNIPAM chain segments. In contrast, we fail to observe the aromatic proton signals of the TP2NH<sub>3</sub><sup>+</sup> species when TP-PNIPAM1 was dispersed in D<sub>2</sub>O (Figure 9B). True dissolution of TP-PNIPAM1 in CD<sub>2</sub>Cl<sub>2</sub> facilitates the detections of all proton resonance bands; however, when micelles form, the hydrophobic luminogens self-assemble into the central core of the micelles and the molecular motions of the TP2NH<sub>3</sub><sup>+</sup> species in the congested core are so highly restricted that their motions can no longer be seen by the <sup>1</sup>H NMR. At this stage, the extended chain segments of the outer PNIPAM shell are free to rotate and the multiple sharp resonances of the main-chain (protons  $H_a$  and  $H_b$ ) and the side-chain (protons  $H_c$ ) protons can be clearly viewed.

When heated to temperatures above LCST, dissociations of hydrogen-bond interactions result in dehydration and contraction of the PNIPAM chain segments, during which, mass aggregations of several collapsed micelles occur to result in the large, globular nanoparticles with diameters >170 nm (cf. Figure 8). At 50 °C (Figure 9D), the contracted PNIPAM chains within the globule have such limited rotation freedom that the resonances peaks of the main- and the side-chain protons broaden in shape and are reduced in magnitude, which are in great contrast to the sharp and large proton resonances observed at 25 and 37 °C (Figure 9, parts B and C).

#### Comparison between TP-PNIPAM $n$ and $Pm$ Systems.

In contrast to the ionic TP-PNIPAM $n$  complexes, the covalently linked TP polymers of  $Pm$ <sup>36</sup> (cf. Scheme 1) exhibit the reverse emission quenching at temperatures higher than LCST. At room temperature, the single TP centers of  $Pm$  associate to each other to form an aggregated core with strong emission. At high temperatures, the aggregated core was broken and isolated by the contracted PNIPAM chains, leading to the disappearance of the AIE-operative emission. For the present TP-PNIPAM $n$  system, the varied high-temperature fluorescence response is attributed to the ionic ammonium sulfonate bonds in between the PNIPAM and the TP2NH<sub>3</sub><sup>+</sup> layers. At room temperature, the phase-separated TP2NH<sub>3</sub><sup>+</sup> core is stabilized by the long-range electrostatic interactions from the

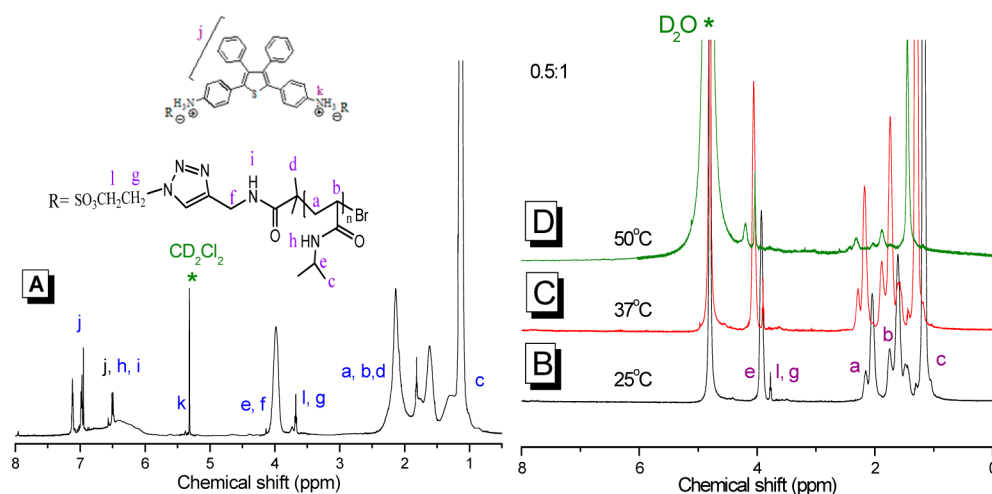


**Figure 9.**  $^1\text{H}$  NMR spectra of TP-PNIPAM1 in (A)  $\text{CD}_2\text{Cl}_2$  at 25 °C and (B–D) in  $\text{D}_2\text{O}$  at various temperatures.

sulfonate counterions. The long-range electrostatic interactions are supposed to be strong and survive at higher temperatures; therefore, at temperatures higher than LCST, the aggregated  $\text{TP}2\text{NH}_3^+$  phase still persists and remains isolated from the PNIPAM chains. During the collapse/aggregation process, the contracted PNIPAM chains act to shrink the phase-separated  $\text{TP}2\text{NH}_3^+$  aggregates, during which molecular rotation of  $\text{TP}2\text{NH}_3^+$  was further restricted to result in the emission intensification. The varied fluorescence responses between  $P_m$  and TP-PNIPAM systems therefore rely on the type of linkages connecting the luminogen and the PNIPAM chain.

#### 4. CONCLUSIONS

The ionic  $\text{TP}2\text{NH}_3^+$  luminogen was prepared to complex with polymeric SECPS to generate three amphiphilic complexes of TP-PNIPAM $n$ . The solution emission behaviors of TP-PNIPAM $n$ s in ethanol/acetone solvent/nonsolvent pair suggest that TP-PNIPAMs are indeed AIE-active materials due to the built-in TP luminogens.

Dilute solutions of TP-PNIPAM $n$  in water are nonemissive; however, above CMC, TP-PNIPAM $n$  chains self-assemble to form micelles with strong emission due to the AIE effect of the aggregated  $\text{TP}2\text{NH}_3^+$  core. The CMC values evaluated from the distinct emission behavior are 0.139, 0.105, and 0.068 mg/mL for TP-PNIPAM1, -2, and -3, respectively.

At temperatures above LCST, dehydrations and contractions of PNIPAM chains result in the coil-to-globule transition. LCSTs evaluated from transmittance and DLS are 48.1, 47.6, and 46.3 °C for TP-PNIPAM1, -2, and -3, respectively. With the highest hydrophobic TP content, TP-PNIPAM3 forms large globular structures at a stage earlier than TP-PNIPAM2 and -1. At 55 °C, all aqueous solutions have higher emission intensities than the intensities measured at room temperature. At high temperatures, the fluorescent  $\text{TP}2\text{PN}_3^+$  aggregated phase is secured by the long-range electrostatic interactions provided by the sulfonate counterions in PNIPAM. However, the contracted PNIPAM chains tend to shrink the  $\text{TP}2\text{NH}_3^+$  aggregates to result in the emission intensification due to the enhanced restriction on molecular rotation.

#### ■ ASSOCIATED CONTENT

##### Supporting Information

A TEM image showing the micelles structure, mass spectra, emission spectra of the aqueous TP-PNIPAM $n$  solutions at different concentrations, and  $^1\text{H}$  NMR spectra of TP-PNIPAM2 and -3 at high temperatures. This material is available free of charge via the Internet at <http://pubs.acs.org>.

#### ■ AUTHOR INFORMATION

##### Corresponding Author

\*E-mail: [jlhong@mail.nsysu.edu.tw](mailto:jlhong@mail.nsysu.edu.tw). Phone: +886-7-5252000, ext. 4065.

##### Notes

Notes. The authors declare no competing financial interest.

#### ■ ACKNOWLEDGMENTS

We appreciate the financial support from National Science Council, Taiwan under contract no. 101-2221-E-110-022.

#### ■ REFERENCES

- (1) Schatz, C.; Louguet, S.; Le Meins, J.-F.; Lecommandoux, S. Polysaccharide-block-polypeptide Copolymer Vesicles: Towards Synthetic Viral Capsids. *Angew. Chem., Int. Ed.* **2009**, *48*, 2572–2575.
- (2) Meng, F.; Zhong, Z.; Feijen, J. Stimuli-Responsive Polymers for Programmed Drug Delivery. *Biomacromolecules* **2009**, *10*, 197–209.
- (3) Vriezema, D. M.; Aragonès, M. C.; Elemans, J. A. A. W.; Cornelissen, J. J. L. M.; Rowan, A. E.; Nolte, R. J. M. Self-Assembled Nanoreactors. *Chem. Rev.* **2005**, *105*, 1445–1490.
- (4) Wang, Y.; Xu, H.; Zhang, X. Tuning the Amphiphilicity of Building Blocks: Controlled Self-Assembly and Disassembly for Functional Supramolecular Materials. *Adv. Mater.* **2009**, *21*, 2849–2864.
- (5) Rapoport, N. Physical Stimuli-Responsive Polymeric Micelles for Anti-Cancer Drug Delivery. *Prog. Polym. Sci.* **2007**, *32*, 962–990.
- (6) Allen, C.; Maysinger, D.; Eisenberg, A. Nano-Engineering Block Copolymer Aggregates for Drug Delivery. *Colloids Surf. B* **1999**, *16*, 3–27.
- (7) Zheng, X. M.; Jiang, T.; He, F. Synthesis and Characterization of PNIPAM-*b*-Polycarbonate copolymers as Self-assembled Thermosensitive Micelles for Drug Delivery. *Acta Polym. Sin.* **2011**, *8*, 895–902.
- (8) Scarpa, J. S.; Mueller, D. D.; Klotz, I. M. Slow Hydrogen-Deuterium Exchange in a Non- $\alpha$ -Helical Polyamide. *J. Am. Chem. Soc.* **1967**, *89*, 6024–6030.
- (9) Schild, H. G. Poly(*N*-isopropylacrylamide): Experiment, Theory and Application. *Prog. Polym. Sci.* **1992**, *17*, 163–249.

- (10) Winnik, F. M. Phase Transition of Aqueous Poly(*N*-isopropylacrylamide) Solutions: a Study by Non-Radiative Energy Transfer. *Polymer* **1990**, *31*, 2125–2134.
- (11) Ringsdorf, H.; Simon, J.; Winnik, F. M. Hydrophobically-Modified Poly(*N*-isopropylacrylamides) in Water: Probing of the Microdomain Composition by Nonradiative Energy Transfer. *Macromolecules* **1992**, *25*, 5353–5361.
- (12) Chee, C. K.; Rimmer, S.; Soutar, I.; Swanson, L. Fluorescence Investigations of the Thermally Induced Conformational Transition of Poly(*N*-isopropylacrylamide). *Polymer* **2001**, *42*, 5079–5087.
- (13) Rimmer, S.; Soutar, I.; Swanson, L. Switching the Conformational Behaviour of Poly(*N*-isopropylacrylamide). *Polym. Int.* **2009**, *58*, 273–278.
- (14) Matsuyama, A.; Tanaka, F. Theory of Solvation-Induced Reentrant Coil-Globule Transition of an Isolated Polymer Chain. *J. Chem. Phys.* **1991**, *94*, 781–786.
- (15) Wu, C.; Zhou, S. Thermodynamically Stable Globule State of a Single Poly(*N*-isopropylacrylamide) Chain in Water. *Macromolecules* **1995**, *28*, 5388–5390.
- (16) Okada, Y.; Tanaka, F. Cooperative Hydration, Chain Collapse, and Flat LCST Behavior in Aqueous Poly(*N*-isopropylacrylamide) Solutions. *Macromolecules* **2005**, *38*, 4465–4471.
- (17) Luo, J.; Xie, Z.; Lam, J. W. Y.; Cheng, L.; Chen, H.; Qiu, C.; Kwok, H. S.; Zhan, X.; Liu, Y.; Zhu, D.; Tang, B. Z. Aggregation-Induced Emission of 1-Methyl-1,2,3,4,5-pentaphenylsilole. *Chem. Commun.* **2001**, 1740–1741.
- (18) Chen, H. Y.; Lam, W. Y.; Luo, J. D.; Ho, Y. L.; Tang, B. Z.; Zhu, D. B.; Wong, M.; Kwok, H. S. Highly Efficient Organic Light-Emitting Diodes with a Silole-Based Compound. *Appl. Phys. Lett.* **2002**, *81*, 574–576.
- (19) Chen, J.; Law, C. C. W.; Lam, J. W. Y.; Dong, Y.; Lo, S. M. F.; Williams, I. D.; Zhu, D.; Tang, B. Z. Synthesis, Light Emission, Nanoaggregation, and Restricted Intramolecular Rotation of 1,1-Substituted 2,3,4,5-Tetraphenylsiloles. *Chem. Mater.* **2003**, *15*, 1535–1546.
- (20) Chen, J.; Xie, Z.; Lam, J. W. Y.; Law, C. C. W.; Tang, B. Z. Silole-Containing Polyacetylenes: Synthesis, Thermal Stability, Light Emission, Nanodimensional Aggregation, and Restricted Intramolecular Rotation. *Macromolecules* **2003**, *36*, 1108–1117.
- (21) Chen, J.; Peng, H.; Law, C. C. W.; Dong, Y.; Lam, J. W. Y.; Williams, I. D.; Tang, B. Z. Hyperbranched Poly(phenylenesilole)s: Synthesis, Thermal Stability, Electronic Conjugation, Optical Power Limiting, and Cooling-Enhanced Light Emission. *Macromolecules* **2003**, *36*, 4319–4327.
- (22) Dong, S.; Li, Z.; Qin, J. New Carbazole-Based Fluorophores: Synthesis, Characterization, and Aggregation-Induced Emission Enhancement. *J. Phys. Chem. B* **2009**, *113*, 434–441.
- (23) Yuan, C. X.; Tao, X. T.; Wang, L.; Yang, J. X.; Jiang, M. H. Fluorescent Turn-On Detection and Assay of Protein Based on Lambda ( $\Lambda$ )-Shaped Pyridinium Salts with Aggregation-Induced Emission Characteristics. *J. Phys. Chem. C* **2009**, *113*, 6809–6814.
- (24) Liu, Y.; Tao, X.; Wang, F.; Dang, X.; Zou, D.; Ren, Y.; Jiang, M. Aggregation-Induced Emissions of Fluorenonearylamine Derivatives: A New Kind of Materials for Nondoped Red Organic Light-Emitting Diodes. *J. Phys. Chem. C* **2008**, *112*, 3975–3981.
- (25) Xu, B.; Chi, Z.; Yang, Z.; Chen, J.; Deng, S.; Li, H.; Li, X.; Zhang, Y.; Xu, N.; Xu, J. Facile Synthesis of a New Class of Aggregation-Induced Emission Materials Derived from Triphenylethylene. *J. Mater. Chem.* **2010**, *20*, 4135–4141.
- (26) Zhao, Z.; Chen, S.; Lam, J. W. Y.; Lu, P.; Zhong, Y.; Wong, K. S.; Kwok, H. S.; Tang, B. Z. Creation of Highly Efficient Solid Emitter by Decorating Pyrene Core with AIE-Active Tetraphenylethene Peripheries. *Chem. Commun.* **2010**, 2221–2223.
- (27) Tang, L.; Jin, J. K.; Qin, A.; Yuan, W. Z.; Mao, Y.; Mei, J.; Sun, J. Z.; Tang, B. Z. A Fluorescent Thermometer Operating in Aggregation-Induced Emission Mechanism: Probing Thermal Transitions of PNIPAM in Water. *Chem. Commun.* **2009**, 4974–4976.
- (28) Liu, J.; Zhong, Y.; Lam, J. W. Y.; Lu, P.; Hong, Y.; Yu, Y.; Yue, Y.; Faisal, M.; Sung, H. H. Y.; Williams, I. D.; Wong, K. S.; Tang, B. Z. Hyperbranched Conjugated Polysiloles: Synthesis, Structure, Aggregation-Enhanced Emission, Multicolor Fluorescent Photopatterning, and Superamplified Detection of Explosives. *Macromolecules* **2010**, *43*, 4921–4936.
- (29) Qin, A.; Lam, J. W. Y.; Tang, L.; Jim, C. K. W.; Zhao, H.; Sun, J.; Tang, B. Z. Polytriazoles with Aggregation-Induced Emission Characteristics: Synthesis by Click Polymerization and Application as Explosive Chemosensors. *Macromolecules* **2009**, *42*, 1421–1424.
- (30) Chien, R. H.; Lai, C. T.; Hong, J. L. Enhanced Aggregation Emission of Vinyl Polymer Containing Tetraphenylthiophene Pendant Group. *J. Phys. Chem. C* **2011**, *115*, 5958–5965.
- (31) Lai, C. T.; Hong, J. L. Aggregation-Induced Emission in Tetraphenylthiophene-Derived Organic Molecules and Vinyl Polymer. *J. Phys. Chem. B* **2010**, *114*, 10302–10310.
- (32) Chou, C. A.; Chien, R. H.; Lai, C. T.; Hong, J. L. Complexation of bulky Camphorsulfonic Acid to Enhance Emission of Organic and Polymeric Fluorophores with Inherent Quinoline Moiety. *Chem. Phys. Lett.* **2010**, *501*, 80–86.
- (33) Hong, Y.; Lam, J. W. Y.; Tang, B. Z. Aggregation-Induced Emission: Phenomenon, Mechanism and Applications. *Chem. Commun.* **2009**, 4332–4353.
- (34) Liu, J.; Lam, J. W. Y.; Tang, B. Z. Aggregation-Induced Emission of Silole Molecules and Polymers: Fundamental and Applications. *J. Inorg. Organomet. Polym.* **2009**, *19*, 249–285.
- (35) Qin, A.; Lam, J. W. Y.; Tang, B. Z. Luminogenic Polymers with Aggregation-Induced Emission Characteristics. *Prog. Polym. Sci.* **2012**, *37*, 182–209.
- (36) Lai, C. T.; Chien, R. H.; Kuo, S. W.; Hong, J. L. Tetraphenylthiophene-Functionalized Poly(*N*-isopropylacrylamide): Probing LCST with Aggregation-Induced Emission. *Macromolecules* **2011**, *44*, 6546–6556.
- (37) Lai, Y.-W.; Kuo, S.-W.; Hong, J.-L. Complexing AIEE-Active Tetraphenylthiophene Fluorophore to Poly(*N*-isopropylacrylamide): Fluorescence Responses toward Acid, Base and Metal ions. *RSC Adv.* **2012**, *2*, 8194–8200.
- (38) Li, H.; Chi, Z.; Zhang, X.; Xu, B.; Liu, S.; Zhang, Y.; Xu, J. New Red Aggregation-Induced Emission Enhancement Compounds with High Thermal Stabilities and Excellent Non-doped Red OLED Performances Were Synthesized. *Chem. Commun.* **2011**, 47, 11273–11275.
- (39) Ruthard, C.; Maskos, M.; Kolb, U.; Gröhn, F. Finite-Size Networks from cylindrical Polyelectrolyte Brushes and Porphyrins. *Macromolecules* **2009**, *42*, 830–840.
- (40) Egawa, Y.; Hayashida, R.; Anzai, J. pH-Induced Interconversion between J-Aggregates and H-Aggregates of 5,10,15,20-Tetrakis(4-sulfonatophenyl)porphyrin in Polyelectrolyte Multilayer Films. *Langmuir* **2007**, *23*, 13146–13150.
- (41) Kubát, P.; Lang, K.; Janda, P.; Anzenbacher, P. Interaction of Porphyrins with a Dendrimer Template: Self-Aggregation Controlled by pH. *Langmuir* **2005**, *21*, 9714–9720.
- (42) Moreno-Villoslada, I.; Fuenzalida, J. P.; Tripailaf, G.; Araya-Hermosilla, R.; Pizarro, G. C.; Marambio, O. G.; Nishide, H. Comparative Study of the Self-Aggregation of Rhodamine 6G in the Presence of Poly(sodium 4-styrenesulfonate), Poly(*N*-phenylmaleimide-*co*-acrylic acid), Poly(styrene-*alt*-maleic acid), and Poly(sodium acrylate). *J. Phys. Chem. B* **2010**, *114*, 11983–11992.
- (43) Moreno-Villoslada, I.; Torres, C.; González, F.; Shibue, T.; Nishide, H. Binding of Methylene Blue to Polyelectrolytes Containing Sulfonate Groups. *Macromol. Chem. Phys.* **2009**, *210*, 1167–1175.
- (44) Chien, R. H.; Lai, J. T.; Hong, J. L. Complexation of tetraphenylthiophene-Derived Ammonium Chloride to Poly(sodium vinylsulfonate) Polyelectrolytes: Aggregation-Induced Emission Enhancement and Long-Range Interaction. *Macromol. Chem. Phys.* **2012**, *213*, 666.
- (45) Tang, W.; Chen, J.; Liu, Z.-T.; Liu, Z.-W. Synthesis and Characterization of Thermo-responsive Poly(*N*-vinyl-2-pyrrolidone)-*block*-poly(*N*-isopropylacrylamide) Micelles. *J. Macromol. Sci., Part A: Pure Appl. Chem.* **2010**, *47*, 1026–1031.

- (46) Shi, L. J.; Zhao, M. W.; Zheng, L. Q. Micelle Formation by *N*-Alkyl-*N*-Methylpyrrolidinium Bromide in Ethylammonium Nitrate. *Colloids Surf. A* **2011**, *392*, 305–312.
- (47) Shinoda, K. *Colloidal Surfactant*; Academic Press: New York, 1963.